SUNBURNING SOLAR RADIATION IN CENTRAL INDIANA

John E. Frederick[1]:   Department of the Geophysical Sciences, University of Chicago, 1950 E. Greyhound Pass, Box 18-199, Carmel, IN 46033 USA

ABSTRACT.   This work combines radiative transfer calculations for clear skies with measurements of ultraviolet sunlight obtained over a range of cloudy-sky conditions to define the sunburning solar irradiances experienced in central Indiana. Clear-sky ultraviolet irradiances undergo a large annual cycle primarily in response to the changing elevation of the sun above the horizon over a year, with a lesser influence from the periodic behavior in atmospheric ozone amounts. Erythema, defined as a reddening of the skin after exposure to solar radiation, can occur in less than one hr under clear, haze-free skies during a 5-hr interval centered on solar noon in October, during a 7-hr window in April, and a nearly 9-hr span in July. Scattering by clouds attenuates the ground-level irradiance to values that can vary erratically over time scales of minutes to hours and from one day to the next. One-fourth of the measured ultraviolet irradiances are 52% or less of the clear-sky value during June, July, and August. At the opposite extreme, one-fourth of the measured irradiances fall between 82% and 100% of the expected clear-sky result. In mid-July near solar noon, the time required for a minimal reddening of the skin varies from a minimum of 14 min under clear skies to 27 min or longer for the 25% of cases with the thickest cloud cover.

Keywords: Ultraviolet, sunburn, solar radiation, erythema

INTRODUCTION

Numerous epidemiological studies conducted over several decades point to a role for solar ultraviolet radiation in the occurrence of skin cancer (e.g., Scotto et al. 1974; Fears & Scotto 1983; Vitasa et al. 1990; Urbach 1991; Wu et al. 2016). In recent years approximately 3.3 million people were treated annually for non-melanoma skin cancer in the United States (Rogers et al. 2015), while the more serious form, melanoma, occurs less frequently, with an estimated 87 thousand cases in the country during 2017 (American Cancer Society 2017). According to data reported to the state cancer registry, residents of Indiana experienced 19.8 cases of melanoma per 100,000 residents in 2014 (U.S. Cancer Statistics Working Group 2017), corresponding to approximately 1,300 cases in a total population of 6.595 million people. Analogous statistics for non-melanoma cancers are not reported to state registries, but given a population of 318.6 million in the United States in 2014, one could estimate that roughly 65,000–70,000 cases of non-melanoma occurred in Indiana during that year, where exposure to the sun's ultraviolet radiation is a major risk factor.

This work addresses the solar ultraviolet radiation levels experienced by residents in central Indiana. The index of biological impact adopted here is erythema, defined as a reddening of lightly-pigmented skin that appears several hours after exposure to radiation. A minor sunburn, quantified as a minimal erythema dose or 1 MED, is short-lived, but ongoing exposure to the sun's ultraviolet emission over periods of years is implicated in the development of the non-melanoma cancers noted above (Giese 1976), while more severe cases of sunburn appear related to the eventual appearance of melanoma (Wu et al. 2016).

Ultraviolet irradiances received at the Earth's surface vary with season, latitude, and time of day owing to the changing path length taken by sunlight through the absorbing and scattering atmosphere. Wavelength-dependent absorption by the ozone contained in a vertical atmospheric column determines the amount of energy absorbed, while molecular scattering in the ultraviolet leads to a substantial diffuse component of irradiance, even when clouds are absent. The ultraviolet irradiance received at ground-level under clear, haze-free skies can serve as a useful benchmark to specify the largest radiation levels encountered at a given time of year. Reliable estimates of clear-sky irradiances come from solving the equations of radiative transfer for suitably-chosen model atmospheres, where the column abundance of ozone is the most important input. Two geographic locations at the same

[1] *Corresponding author:* John E. Frederick, 312-213-7185 (phone), frederic@uchicago.edu.

latitude will experience similar clear-sky irradiances, with small differences arising from changes in surface elevation. Although irradiances under clear-skies provide important reference values, a realistic description of the radiation environment must include attenuation by clouds and haze, and this is a primary cause of differences in climatological irradiance received at sites situated at the same latitude. Given the complex spatial and temporal variability of cloudiness, an empirical, statistical approach is necessary to include these effects in a realistic climatology of ultraviolet radiation for a specific geographic region such as central Indiana.

COMPUTED SOLAR IRRADIANCES

The clear-sky calculations reported in this work utilize a one-dimensional model which solves the radiative transfer equations for the downward scattered solar irradiance incident on the ground as a function of wavelength. The total downward spectral irradiance at wavelength λ reaching the Earth's surface, $dE_{TOT}(\lambda,\theta)/d\lambda$, defined as the energy striking unit horizontal area in unit time per unit wavelength interval in $W\,m^{-2}\,nm^{-1}$, is the sum of direct and scattered contributions computed with the sun at angle θ from the local zenith for the latitude, longitude, and local time of interest:

$$dE_{TOT}(\lambda,\theta)/d\lambda = dE_{DIR}(\lambda,\theta)/d\lambda \\ + dE_{SCT}(\lambda,\theta)/d\lambda \quad (1)$$

where $dE_{DIR}(\lambda,\theta)/d\lambda$ is the direct attenuated spectral irradiance and $dE_{SCT}(\lambda,\theta)/d\lambda$ is the scattered irradiance, including all orders of multiple Rayleigh scattering. An application of Beer's Law produces the direct component of solar irradiance. The scattered component is obtained by solving the one-dimensional radiative transfer equations for both upward and downward irradiance. The singly and multiply scattered radiation fields are assumed to be isotropic over a hemisphere, leading to the equations presented by Frederick & Lubin (1988).

The calculation includes absorption by atmospheric ozone, with the column amount specified from satellite observations. The lower boundary of the atmosphere is a Lambertian surface whose albedo is set to 0.2, where this value is derived from simultaneous upward and downward solar irradiance measurements made over a grass-covered surface in Hamilton County, Indiana. Additional inputs to the calculation are the
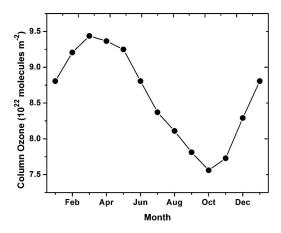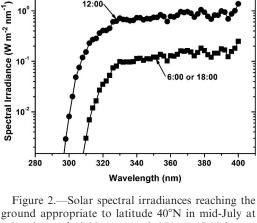

Figure 1.—Annual cycle in column ozone abundance for latitude 40°N appropriate to central Indiana.

extraterrestrial solar irradiance at wavelengths from 290 to 400 nm for an Earth-sun distance of one astronomical unit, cross sections for Rayleigh scattering, and absorption cross sections for ozone. The model adjusts the input extraterrestrial irradiances based on the day of the year to include the varying Earth-sun distance. The literature includes descriptions of similar models (Frederick & Lubin 1988) and of the required input parameters (Frederick et al. 1985) so that no further description of the mathematical development is needed here.

The adopted column ozone amounts are appropriate to latitude 40°N, which passes through the southern portion of Hamilton County, Indiana. The dataset from NASA's Total Ozone Mapping Spectrometer (TOMS) on the Earth Probe satellite (Antón et al. 2010) is available in a format well-suited for developing the required climatology. The values used here are averages of all data obtained between 39°N and 41°N in one-month time periods over the years 2000 to 2005, the end of the instrument's operation. When averaged over these years, column ozone amounts in longitude bins 1.25° wide situated over Indiana were within 2% or less of the global zonal-mean values for each month. The final ozone climatology used here is based on the global zonal means. Figure 1 displays the monthly ozone abundances expressed as the number of molecules in a vertical column whose cross sectional area is $1\,m^2$. The column amounts display the well-known annual cycle (Bojkov & Fioletov 1995) created by transport processes at stratospheric altitudes, with maximum ozone

Figure 2.—Solar spectral irradiances reaching the ground appropriate to latitude 40°N in mid-July at solar times of 12:00 noon and 6:00 or 18:00 hours. Values refer to clear skies.

Figure 3.—Ratio of scattered irradiance to total spectral irradiance reaching the ground for latitude 40°N under clear skies in mid-July.

values appearing in spring and a minimum in autumn. The column density in March is nearly 25% larger than the result for October, with a decline taking place over the summer months. This seasonal behavior acts to shift the maximum in sunburning ultraviolet irradiances from the solstice near June 21 into early July.

Figure 2 presents the computed solar spectral irradiance $dE_{TOT}(\lambda,\theta)/d\lambda$ as a function of wavelength from 290 nm to 400 nm under clear, haze-free skies. Values refer to mid-July at 12:00 noon solar time and at times displaced six hours on either side of solar noon, 6:00 and 18:00 hours, where noon solar time is defined by the solar zenith angle θ having its minimum value for the day. Note the logarithmic scale and the steep decline in spectral irradiance due to absorption by ozone as wavelength decreases from 320 nm to 300 nm. The dependence on solar time traces to a changing path length taken by radiation through the absorbing atmosphere over the daylight period. For the direct component of irradiance an additional factor arises from a geometrical effect where a fixed amount of energy is spread over a larger horizontal area as the angle of incidence θ from the vertical increases.

Figure 3 shows the relative contributions of scattered radiation to the totals in Fig. 2 by plotting the ratio of scattered irradiance to total irradiance as a function of wavelength. Figure 3 omits any influence by clouds and haze, and it thereby depicts the minimum possible contribution from scatering. For solar noon conditions, scattered radiation varies from 22% of the total at
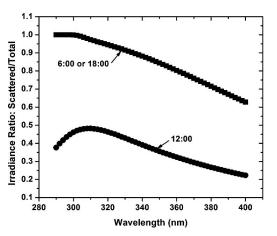
400 nm to a maximum of 48% near 310 nm. The decline toward still shorter wavelengths is a consequence of increasingly strong absorption by ozone at $\lambda < 310$ nm. The effective atmospheric path length taken by scattered radiation is longer than that of direct radiation for small solar zenith angles, and this leads to a greater absorption of the scattered component. For solar zenith angles in early morning and late afternoon, 6:00 and 18:00 hours, the scattered component of irradiance is larger on a relative basis than during mid-day hours and varies from 63% of the total irradiance at 400 nm to 99 percent or more for $\lambda < 305$ nm.

The effectiveness of solar radiation in causing erythema varies with wavelength, where the "biologically effective" spectral irradiance $dE_{EFF}(\lambda,\theta)/d\lambda$ is related to the actual spectral irradiance by:

$$dE_{EFF}(\lambda, \theta)/d\lambda = A(\lambda)dE_{TOT}(\lambda, \theta)/d\lambda \quad (2)$$

where $A(\lambda)$ is the dimensionless action spectrum for erythema which, by convention, is normalized to 1.0 at its maximum (McKinlay & Diffey 1987). Figure 4 presents $A(\lambda)$ based on the analytic expression presented in Webb et al. (2011). Note the negative correlation with ground-level irradiance where biological effectiveness is large at wavelengths where spectral irradiance is small. Figure 5 illustrates the biologically effective spectral irradiance in mid-July for the solar times from Fig. 2. Between 12:00 and 6:00/18:00 hours solar time the largest biologically effective spectral irradiances shift in wavelength from 300–310 nm
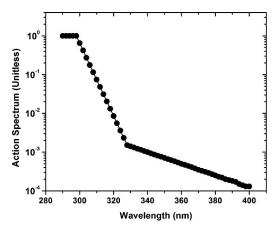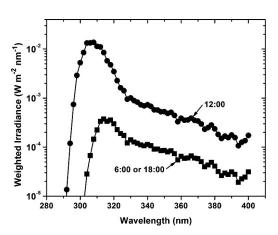
Figure 4.—Action spectrum for erythema over the wavelength range 290–400 nm. Values are normalized to 1.0 for wavelengths shorter than 300 nm and set to 0.0 at wavelengths longer than 400 nm.

to 310–320 nm, and the absolute value declines to less than 3% of the noon maximum. The shift in the peak is a consequence of the wavelength-dependent absorption by ozone. When the atmospheric path length taken by sunlight is relatively long, the shortest ultraviolet wavelengths are preferentially depleted, thereby shifting the maximum in biologically effective irradiance.

The total biologically effective irradiance in J m^{-2} s^{-1} is:

$$E_{EFF} = \int d\lambda A(\lambda) dE_{TOT}(\lambda)/d\lambda \qquad (3)$$

Figure 5.—Biologically-weighted spectral irradiances for latitude 40°N in mid-July at solar times of 12:00 noon and 6:00 or 18:00 hours. Values refer to clear skies.
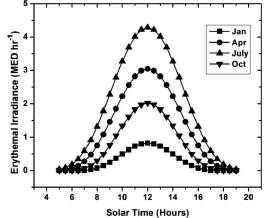

Figure 6.—Variation in ground-level erythemal irradiance with solar time under clear skies at 40°N. Curves from highest irradiance to lowest refer to mid-July, mid-April, mid-October, and mid-January in units of MED hr^{-1}.

where the integral extends over wavelength from λ = 290 nm, below which $dE_{TOT}(\lambda)/d\lambda$ is negligibly small, to λ = 400 nm, above which $A(\lambda)$ = 0.0. For health-related and medical applications, a convenient unit is the number of Minimal Erythema Doses (MED) per hour. This measure adopts the definition of 1 MED as the radiation dose that leads to an observable reddening of fair skin, typically taken as equivalent to a time-integrated dose equal to 210 J m^{-2} of biologically effective radiation as defined in Equation 3 (Pathak & Fanselow 1983). The biologically effective irradiance in MED hr^{-1}, E_{MED}, is simply E_{EFF} multiplied by (3600 s hr^{-1})/(210 J m^{-2} MED^{-1}). The quantity E_{MED} is hereafter referred to as the "erythemal irradiance."

Figure 6 illustrates the variation in erythemal irradiance striking a horizontal surface with season and solar time under clear, haze-free skies. Note that for the longitude of Indianapolis, solar noon occurs approximately 1.8 hours after local noon Eastern Daylight Time in summer. The four curves refer to January 16, April 16, July 16, and October 16. The differences between months arise primarily from different solar zenith angles, with seasonal changes in column ozone and in the Earth-sun distance being secondary factors. The peak erythemal irradiances at solar noon are 4.3 MED hr^{-1} in July, 3.0 MED hr^{-1} in April, 2.0 MED hr^{-1} in October, and 0.8 MED hr^{-1} in January. The time required for a horizontal surface to receive a dose equivalent to 1 MED

Figure 7.—Time required for a horizontal surface to receive a radiation dose of 1 MED under clear skies at latitude 40°N. Curves from shortest time to longest refer to mid-July, mid-April, mid-October, and mid-January. Horizontal lines denote times of 120, 90, 60 and 30 minutes.

Figure 8.—Erythemal irradiances measured at 10-min intervals during a nearly-clear day and a day with thick and variable cloudiness, July 25 and July 10, 2017, respectively.

under clear skies is a medically-relevant measure of the radiation field. Figure 7 presents this time in minutes for the four months shown in Fig. 6. Dashed horizontal lines in Fig. 7 denote 30, 60, 90, and 120 min. Times-to-1 MED equal to or shorter than 30 min exist in October, April, and July, while substantial portions of the daylight period during these months have times less than one hour. In July, the month of highest ultraviolet radiation levels, the time-to-1 MED is less than 30 min for nearly 7 hr centered on solar noon.

ATTENUATION BY CLOUDS AND HAZE

The clear-sky erythemal irradiances presented above are limiting cases; the actual radiation levels encountered at any location depend on the characteristics of haze and cloudiness, and these can vary substantially from one geographic location to another and with time. The range of possible cloud geometries and thicknesses motivates an empirical approach to incorporating the influence of haze and cloudiness into estimates of climatological radiation exposure. This work uses a dataset obtained by a Davis Instruments Ultraviolet Radiation Sensor, Model 6490, over the period June 2015 through August 2017 to describe the attenuation of erythemal irradiance by clouds and haze in central Indiana. The sensor is located at latitude 40.0°N, longitude 86.1°W in southern Hamilton County, Indiana. The instrument has a spectral response function similar to the action spectrum for erythema in Fig. 4, and it
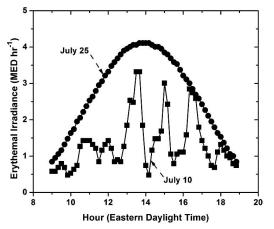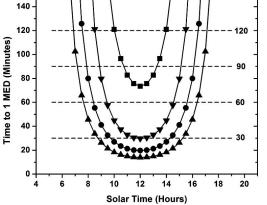
records one measurement comparable to the result of Equation 3 every 10 min. The manufacturer estimates an absolute accuracy of ± 5%. The present work uses the ratio of measured irradiance to clear-sky irradiance at the same solar zenith angle, where both quantities are inferred from the sensor, so that systematic offsets in calibration tend to cancel. The objective is to characterize the attenuation provided by clouds and haze in a statistical sense for time periods measuring three months in duration. The use of a large number of measurements to produce statistical summaries acts to minimize the effect of random errors. Figure 8 presents measured erythemal irradiances for two days, where the sensor's output is converted to MED hr^{-1} for consistency with calculated values. July 25, 2017 was a nearly-clear day, while thick, variable cloudiness prevailed on July 10, 2017. Note that the horizontal scale is Eastern Daylight Time (EDT) where solar noon at the longitude of the sensor occurs near 1:45–1:50 PM EDT. The rapid variations in erythemal irradiance associated with changing cloudiness are apparent.

Figure 9 includes all irradiances measured during June, July, and August during three summer seasons from 2015 through 2017 plotted against solar zenith angle θ for θ ≤ 60°. This is $E_{MS}(i,\theta)$ where i=1,2,..., labels individual data points expressed in W m^{-2} with the normalized action spectrum implicit in the reported values. The upper envelope corresponds to cloud-free conditions with minimal haze and provides the
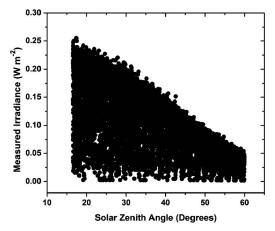
Figure 9.—Erythemal irradiances measured during June, July, and August of 2015, 2016 and 2017 plotted against the corresponding solar zenith angles. The upper envelope defines clear, haze-free skies. (W m^{-2} = watt per meter squared)

basis for defining a clear-sky reference $E_{CLR}(\theta)$ as a function of θ. The quantity:

$$R(i, \theta) = E_{MS}(i, \theta)/E_{CLR}(\theta) \qquad (4)$$

characterizes the influence of clouds and haze on the ith irradiance. The measured and clear-sky irradiances vary with solar elevation in essentially the same way, so the dependence on θ tends to cancel in the ratio. The histogram of R-values in Fig. 10 summarizes the influence of clouds and haze for the entire dataset, June 2015–August 2017, where a total of 26,982 measurements enter the plot. Completely clear skies, with R approximately equal to 1.0, are infrequent, although 48% of the measurements correspond to R $\geq$ 0.75. Relatively thick cloud cover, with R $\leq$ 0.50, occurs in 27% of the observations.

IRRADIANCES INCLUDING CLOUDINESS

The approach developed here allows including the statistical properties of local cloudiness into estimates of erythemal irradiance while avoiding the need to treat the complex behavior evident during cloudy periods. It is convenient to sort the data according to meteorological seasons, where winter encompasses December, January and February, spring includes March, April, and May, summer is June, July, and August, and autumn refers to September, October, and November. Note that the clear-sky calculations shown in
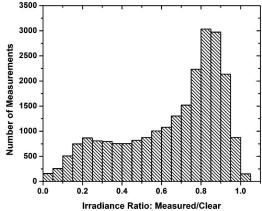

Figure 10.—Histogram of measured-to-clear-sky irradiance ratios derived for solar zenith angles less than 60° over the duration of the dataset, June 2015 through August 2017.

Fig. 6 refer to dates at the center of each meteorological season. Table 1 and Fig. 11 summarize the influence of clouds and haze on erythemal irradiance for each season by giving the median value of R, labeled R(50%), the ratio that defines the upper boundary of the smallest quartile of R-values, R(25%), and the ratio that defines the lower boundary of the largest quartile, R(75%). Clouds have the least influence on erythemal irradiance in meteorological autumn, when the median irradiance is equal to 82% of the clear-sky value and the middle half of values lies between 56% and
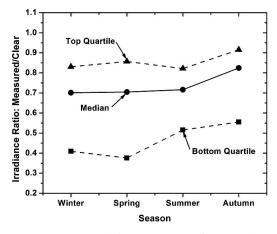

Figure 11.—Statistical summary of attenuation provided by cloudy skies for each season. Solid line defines the median values of the irradiance ratio R=E_{MS}/E_{CLR}. Dashed lines refer to boundaries of the top and bottom quartiles.

Table 1.—Influence of cloudy skies on erythemal irradiance based on the irradiance ratio $R = E_{MS}/E_{CLR}$. R(25%) defines the upper bound of the smallest quartile of irradiance ratios; R(50%) is the median; R(75%) is the lower limit of the largest quartile.

Season (Months)	# Points	R(25%)	R(50%)	R(75%)
Winter (Dec-Jan-Feb)	1,312	0.41	0.70	0.83
Spring (Mar-Apr-May)	7,744	0.38	0.70	0.86
Summer (Jun-Jul-Aug)	13,883	0.52	0.72	0.82
Autumn (Sep-Oct-Nov)	4,043	0.56	0.82	0.92

92% of that for a clear sky. In meteorological summer, the period of largest absolute irradiances, the median is 72% and the interquartile range spans 52% to 82% of the clear-sky values. Similar attenuations occur in winter and spring with median irradiances at 70% of clear-sky levels and interquartile ranges extending from 38–41% to 83–86%.

To estimate biologically effective radiation levels actually experienced in central Indiana, the computed clear-sky erythemal irradiances must be scaled by the fractions in Table 1. The four panels of Fig. 12 present the final distributions for winter, spring, summer, and autumn, where the top curve in each panel is the clear-sky case. At a fixed solar time 25% of the erythemal
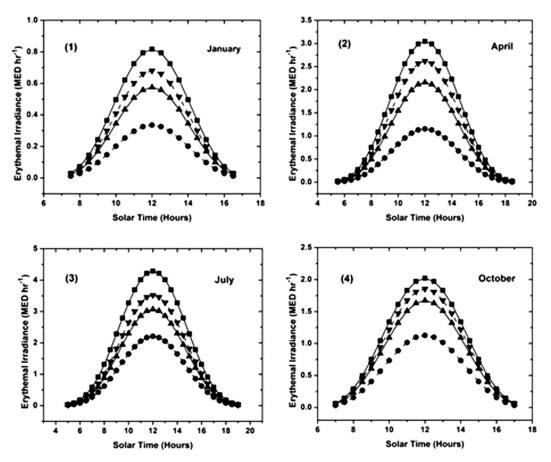

Figure 12.—Erythemal irradiance versus solar time including the influence of cloudiness. The curves, from highest to lowest, refer to clear skies, the lower boundary of the largest quartile of irradiances, the median value, and the upper boundary of the smallest quartile: (1) mid-January, (2) mid-April, (3) mid-July, (4) mid-October.

Table 2.—Time required for a horizontal surface to receive erythemal irradiance equal to 1 MED under cloudy skies typical of central Indiana: Based on irradiances for 12:00 noon and 9:00 or 15:00 hours solar time.

Season	Shortest 25% of cases	Second 25% of cases	Third 25% of cases	Longest 25% of cases
Time (Minutes): 12:00 Hours Solar Time				
Winter	73–88	88–104	104–179	> 179
Spring	20–23	23–28	28–52	> 52
Summer	14–17	17–20	20–27	> 27
Autumn	30–32	32–36	36–53	> 53
Time (Minutes): 9:00 or 15:00 Hours Solar Time				
Winter	247–301	301–357	357–613	> 613
Spring	41–49	49–61	61–115	> 115
Summer	26–32	32–37	37–51	> 51
Autumn	80–89	89–99	99–148	> 148

irradiances encountered during the season lie between two adjacent curves or, when thick clouds are present, beneath the bottom curve in each figure. With summer, July 16 at solar noon, as the most important case, the largest 25% of erythemal irradiances fall between 3.5 and 4.3 MED hr^{-1}, the next 25% fall in the range 3.1 to 3.5 MED hr^{-1}, the next 25% lie between 2.2 and 3.1 MED hr^{-1}, and the smallest 25% are less than 2.2 MED hr^{-1}.

Table 2 presents the times required for a horizontal surface to receive a dose of 1 MED on a day at the midpoint of each meteorological season, including the climatological influence of clouds and haze. Values appear for solar times of 12:00 noon and 9:00/15:00 hours. The times-to-1 MED appear as four ranges corresponding to the shortest 25% to the longest 25% based on the statistical occurrence of different degrees of cloudiness. The times-to-1 MED for summer, mid-July at solar noon, range from 14–17 min in the shortest quartile of cases to greater than 27 min for the longest quartile characterized by the greatest attenuation by clouds. Even in midmorning and mid-afternoon, the time-to-1 MED in July is less than one hour in more than 75% of the cases. Essentially the same 75% probability applies to noontime conditions in mid-April and mid-October.

The values in Table 2 serve as a guide in estimating safe exposure times to erythemal radiation in central Indiana over seasonal time scales. However, as shown by Figure 8, erythemal irradiances encountered on any given day can be highly variable over periods of hours. Given the rapid variations in irradiance that can occur when clouds are present, it is reasonable that plans for outdoor activity err on the side of caution and assume times-to-1 MED appropriate to clear skies.

ACKNOWLEDGMENTS

LITERATURE CITED

American Cancer Society. 2017. Cancer Facts and Figures 2017. American Cancer Society, Atlanta, Georgia. 74 pp.

Antón, M., M.E. Koukouli, M. Kroon, R.D. McPeters, G.J. Labow, D.Balis & A. Serrano. 2010. Global validation of empirically corrected EP-Total Ozone Mapping Spectrometer (TOMS) total ozone columns using Brewer and Dobson ground-based measurements. Journal of Geophysical Research: Atmospheres 115:D19305.

Bojkov, R.D. & V. Fioletov. 1995. Estimating the global ozone characteristics during the last 30 years. Journal of Geophysical Research: Atmospheres 100:16,537–16,551.

Fears, T.R. & J. Scotto. 1983. Estimating increases in skin cancer morbidity due to increases in ultraviolet radiation exposure. Cancer Investigations 1:119–126.

Frederick, J.E., C. Leovy, D.E. Anderson, Jr., G.P. Anderson, R.E. Dickinson, S.R. Drayson, S. Fels, L.A. Hall, J. Kiehl, J.E. Mentall, G.H. Mount, M. Nicolet, C.D. Rodgers, G. Rottman & P.C. Simon. 1985. Chapter 7. Radiative Processes: Solar and Terrestrial. Pp. 349–392. In Atmospheric Ozone 1985: Assessment of our Understanding of the Processes Controlling its Present Distribution and Change. Volume I. Global Ozone Research and Monitoring Project. Report No. 16. World Meteorological Organization, Geneva, Switzerland.

Frederick, J.E. & D. Lubin. 1988. The budget of biologically active ultraviolet radiation in the Earth-atmosphere system. Journal of Geophysical Research: Atmospheres 93:3825–3832.

Giese, A.C. 1976. Living with Our Sun's Ultraviolet Rays. Plenum Press, New York, New York. 185 pp.

McKinlay, A.F. & B.L. Diffey. 1987. A reference spectrum for ultraviolet induced erythema in human skin. CIE-Journal 6:17–22.

Pathak, M.A. & D.L. Fanselow. 1983. Photobiology of melanin pigmentation: dose/response of skin to sunlight and its contents. Journal of the American Academy of Dermatology 9:724–733.

Rogers, H.W., M.A. Weinstock, S.R. Feldman & B.M. Coldiron. 2015. Incidence estimate of non-melanoma skin cancer (keratinocyte carcinomas) in the US population, 2012. Journal of the American Medical Association, Dermatology 151:1081–1086.

Scotto, J., A.W. Kopf & F. Urbach. 1974. Non-melanoma skin cancer among Caucasians in four areas of the United States. Cancer 34:1333–1338.

U.S. Cancer Statistics Working Group. 2017. United States Cancer Statistics: 1999–2014, Incidence and Mortality Web-based Report. Department of Health and Human Services, Centers for Disease Control and Prevention. Atlanta, Georgia. At: http://www.cdc.gov/uscs (Accessed 25 August 2017).

Urbach, F. 1991. Solar ultraviolet radiation and skin cancer in man. Pp. 705–714. *In* Photobiology - The Science and its Applications. (E. Riklis, Ed.). Springer US, New York, New York.

Vitasa, B.C., H.R. Taylor, P.T. Strickland, F.S. Rosenthal, S. West, H. Abbey, S.K. Ng, B. Munoz & E.A. Emmett. 1990. Association of non-melanoma skin cancer and actinic keratosis with cumulative solar ultraviolet exposure in Maryland watermen. Cancer 65:2811–2817.

Webb, A.R., H. Slape, P. Koepke & A.W. Schmal-wieser. 2011. Know your standard: clarifying the CIE action spectrum. Photochemistry and Photobiology 87:483–486.

Wu, S., E. Cho, W-Q. Li, M.A. Weinstock, J. Han & A.A. Qureshi. 2016. History of severe sunburn and risk of skin cancer among women and men in 2 prospective cohort studies. American Journal of Epidemiology 183:824–833.